Angewandte Chemie
Eine Zeitschrift der Gesellschaft Deutscher Chemiker

Supporting Information

69451 Weinheim, Germany

Gold Carbenoids: Lessons Learnt from a Transmetalation Approach**

*Günter Seidel, Barbara Gabor, Richard Goddard, Berit Heggen, Walter Thiel, and Alois Fürstner**

anie_201308842_sm_miscellaneous_information.pdf

Crystallographic Summary

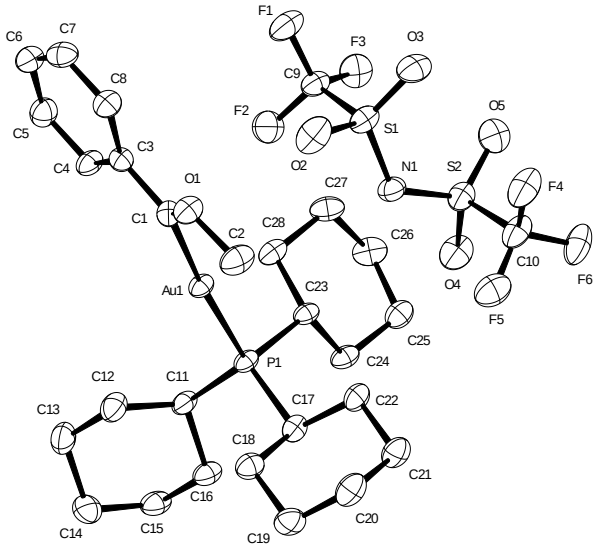

Figure S-1 Structure of complex **8** in the solid state. The anisotropic displacement parameters are drawn at the 50% probability level; hydrogen atoms are omitted for clarity.

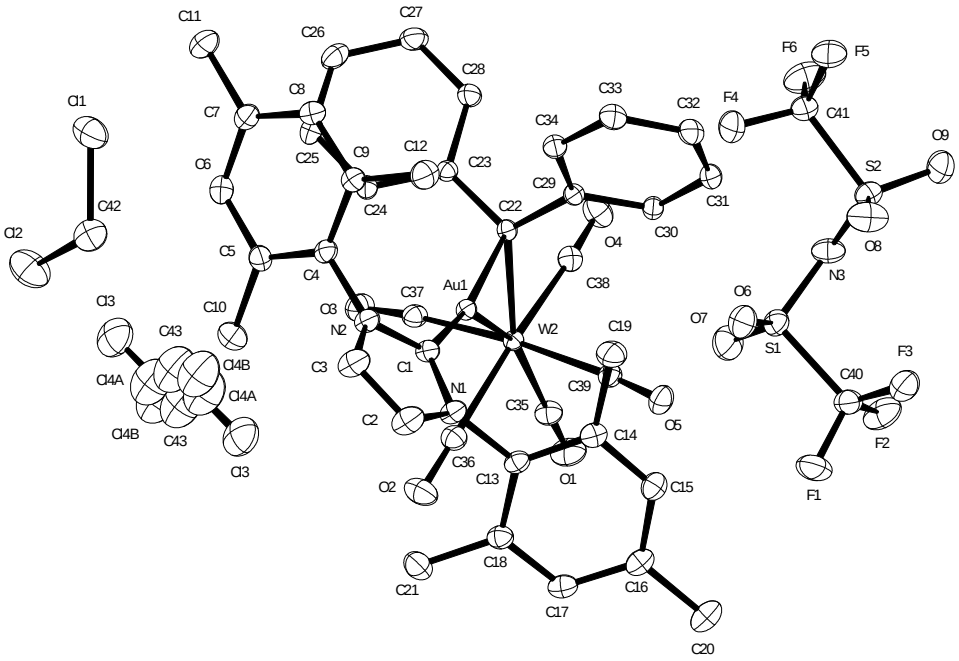

Figure S-2 Structure of complex **10** (L = IMes) in the solid state. The anisotropic displacement parameters are drawn at the 50% probability level; hydrogen atoms are omitted for clarity.

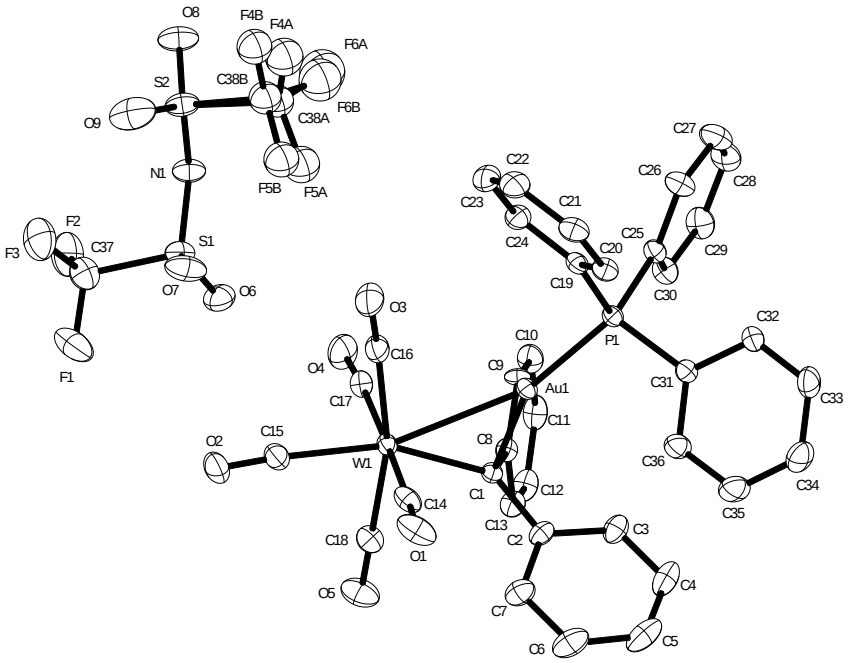

Figure S-3 Structure of complex **10** (L = PPh_3) in the solid state. The anisotropic displacement parameters are drawn at the 50% probability level; hydrogen atoms are omitted for clarity.

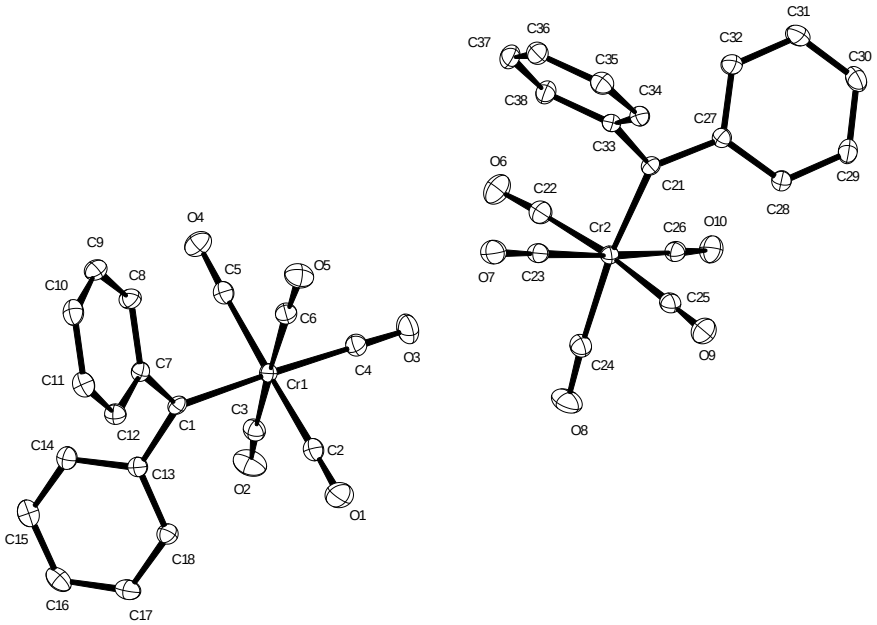

Figure S-4 Structure of complex **12** in the solid state. The anisotropic displacement parameters are drawn at the 50% probability level; hydrogen atoms are omitted for clarity.

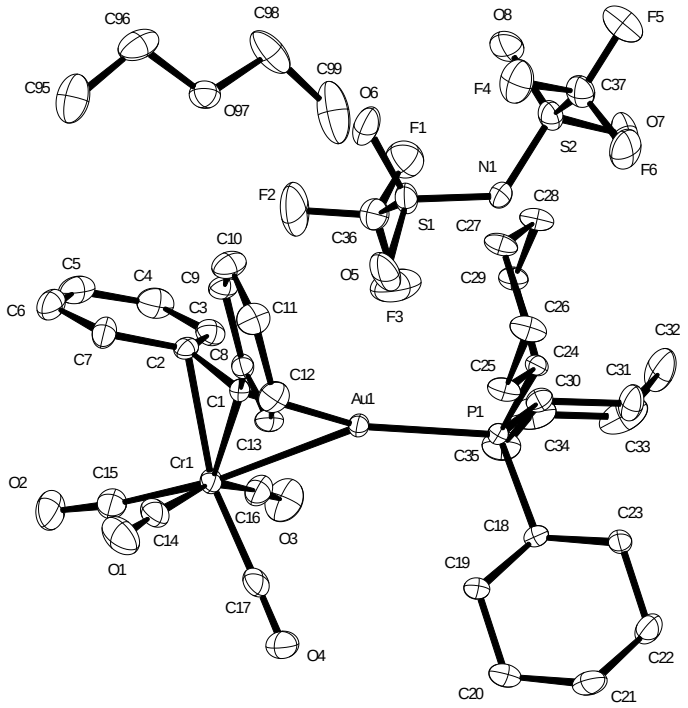

Figure S-5 Structure of complex **14** (L = PCy_3) in the solid state. The anisotropic displacement parameters are drawn at the 50% probability level; hydrogen atoms are omitted for clarity.

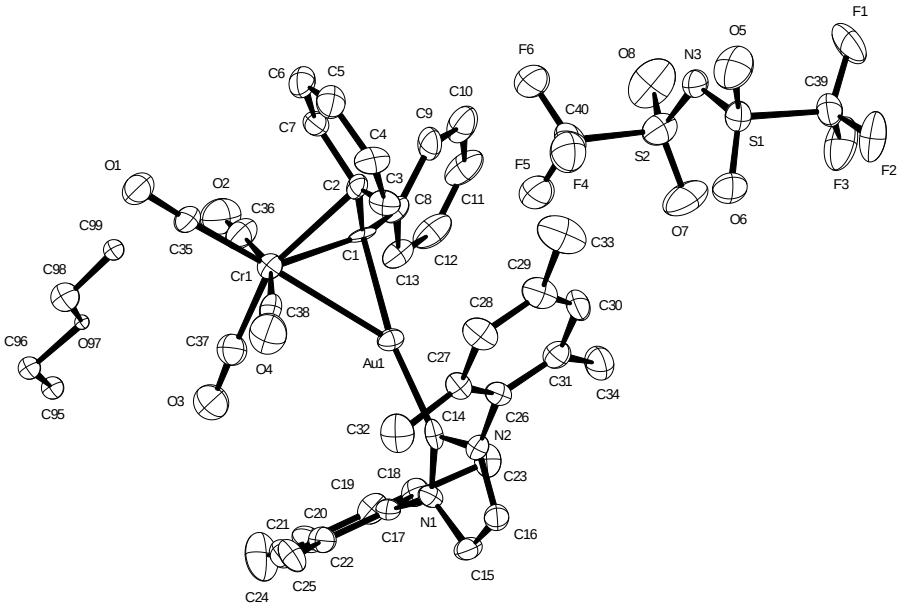

Figure S-6 Structure of complex **14** (L = IMes) in the solid state. The anisotropic displacement parameters are drawn at the 50% probability level; hydrogen atoms are omitted for clarity.

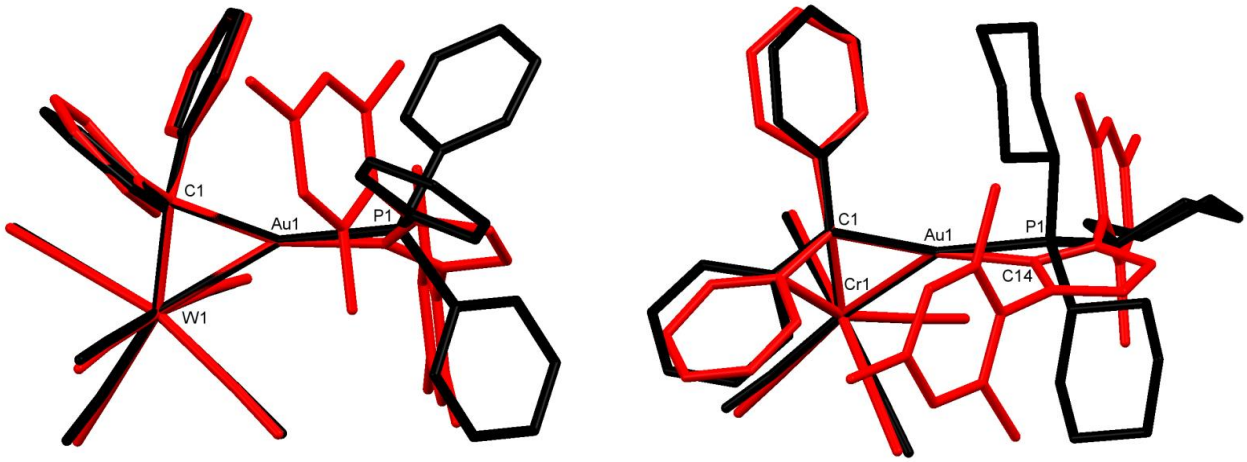

Figure S-7 Left: Superposition of the W, C1 and Au atoms in cations **10** (L = IMes) (red) and **10** (L = PPh_3) (black). Right: Superposition of the Cr, C1 and Au atoms in cations **14** (L = IMes) (red) and **14** (L = PCy_3) (black). In both cases, the L-Au vector with L = IMes (red) points more towards the group-6 metal carbene, indicating more affinity of $(IMes)Au^+$ for the carbene C atom.

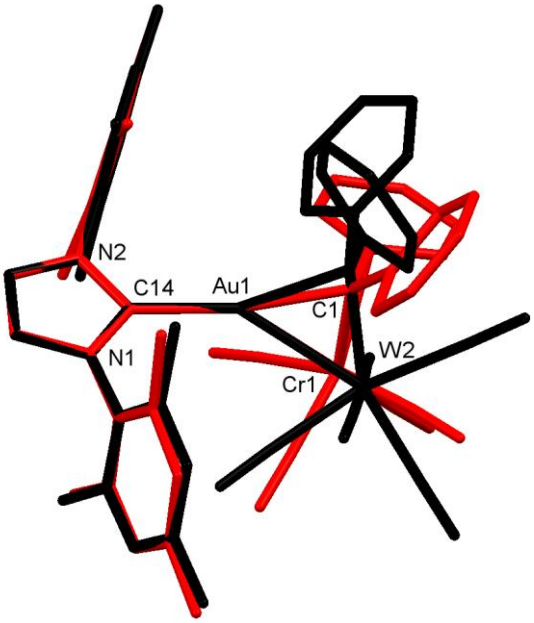

Figure S-8 Superposition of the imidazolylidene-gold moieties in the cations **10** (L = IMes) (red) and **14** (L = IMes) (black), showing better stabilization of the gold carbenoid by the $Cr(CO)_4$ unit.

X-ray Crystal Structure Analysis of Complex 8: $C_{28}H_{41}AuF_6NO_5PS_2$, M_r = 877.67 g · mol^{-1}, red-orange plate, crystal size 0.17 x 0.09 x 0.05 mm, monoclinic, space group $P2_1/n$, a = 11.4858(11) Å, b = 18.674(2) Å, c = 15.5774(10) Å, β = 92.662(6)°, V = 3337.5(6) Å^3, T = 100 K, Z = 4, D_{calc} = 1.747 g·cm^3, λ = 0.71073 Å, μ(*Mo-K*$_\alpha$) = 4.652 mm^{-1}, Gaussian absorption correction (T_{min} = 0.45, T_{max} = 0.80), Bruker-

AXS Enraf-Nonius KappaCCD diffractometer, $2.62 < \theta < 27.50°$, 60543 measured reflections, 7662 independent reflections, 6223 reflections with $I > 2\sigma(I)$, Structure solved by direct methods and refined by full-matrix least-squares against F^2 to $R_1 = 0.039$ [$I > 2\sigma(I)$], $wR_2 =$ 0.118, 398 parameters, H atoms riding, $S =$ 1.154, residual electron density 2.9 / -3.1 e Å^{-3}.

X-ray Crystal Structure Analysis of Complex 10 (L = IMes): $C_{85}H_{74}Au_2Cl_6F_{12}N_6O_{18}S_4W_2$, $M_r = 2798.07$ g · mol^{-1}, black plate, crystal size 0.302 x 0.140 x 0.130 mm, monoclinic, space group $P2_1/c$, $a =$ 10.4897(9) Å, $b =$ 27.399(2) Å, $c =$ 16.9429(15) Å, $\beta =$ 90.962(1)°, $V =$ 4868.8(7) Å^3, $T =$ 100 K, $Z = 2$, $D_{calc} =$ 1.909 g·cm^3, $\lambda =$ 0.71073 Å, μ(*Mo-K*$_\alpha$) = 5.699 mm^{-1}, Gaussian absorption correction ($T_{min} =$ 0.40, $T_{max} =$ 0.69), Bruker-AXS Smart APEX-II diffractometer, $1.94 < \theta < 36.32°$, 185558 measured reflections, 23451 independent reflections, 21511 reflections with $I > 2\sigma(I)$, Structure solved by direct methods and refined by full-matrix least-squares against F^2 to $R_1 = 0.020$ [$I > 2\sigma(I)$], $wR_2 =$ 0.045, 625 parameters, H atoms riding, $S =$ 1.110, residual electron density 2.0 (0.7 Å from Au1) / -1.4 e Å^{-3}.

X-ray Crystal Structure Analysis of Complex 10 (L = PPh$_3$): $C_{38}H_{25}AuF_6NO_9PS_2W$, $M_r = 1229.50$ g · mol^{-1}, black plate, crystal size 0.08 x 0.07 x 0.04 mm, triclinic, space group $P\bar{1}$, $a =$ 12.4337(15) Å, $b =$ 13.5347(16) Å, $c =$ 14.3815(17) Å, $\alpha =$ 86.449(2)°, $\beta =$ 66.011(2)°, $\gamma =$ 64.451(2)°, $V =$ 1976.0(4) Å^3, $T =$ 100 K, $Z = 2$, $D_{calc} =$ 2.066 g·cm^3, $\lambda =$ 0.71073 Å, μ(*Mo-K*$_\alpha$) = 6.847 mm^{-1}, Gaussian absorption correction ($T_{min} =$ 0.35, $T_{max} =$ 0.82), Bruker-AXS Smart APEX-II diffractometer, $2.45 < \theta < 33.73°$, 68391 measured reflections, 15745 independent reflections, 13563 reflections with $I > 2\sigma(I)$, Structure solved by direct methods and refined by full-matrix least-squares against F^2 to $R_1 = 0.023$ [$I > 2\sigma(I)$], $wR_2 =$ 0.059, 529 parameters, H atoms riding, $S =$ 1.020, residual electron density 4.6 (0.85 Å from Au1) / -1.2 e Å^{-3}.

X-ray Crystal Structure Analysis of Complex 12: $C_{18}H_{10}CrO_5$, $M_r = 358.26$ g · mol^{-1}, red plate, crystal size 0.16 x 0.13 x 0.04 mm, triclinic, space group $P\bar{1}$, $a =$ 11.0340(13) Å, $b =$ 12.8200(15) Å, $c =$ 13.043(3) Å, $\alpha =$ 101.328(3)°, $\beta =$ 98.862(3)°, $\gamma =$ 114.167(2)°, $V =$ 1592.8(4) Å^3, $T =$ 100 K, $Z = 4$, $D_{calc} =$ 1.494 g·cm^3, $\lambda =$ 0.71073 Å, μ(*Mo-K*$_\alpha$) = 0.742 mm^{-1}, Gaussian absorption correction ($T_{min} =$ 0.89, $T_{max} =$ 0.97), Bruker-AXS Smart APEX-II diffractometer, $1.65 < \theta < 31.21°$, 47296 measured reflections, 10266 independent reflections, 8511 reflections with $I > 2\sigma(I)$, Structure solved by direct methods and refined by full-matrix least-squares against F^2 to $R_1 = 0.031$ [$I > 2\sigma(I)$], $wR_2 =$ 0.083, 433 parameters, H atoms riding, $S =$ 1.041, residual electron density 0.5 / -0.7 e Å^{-3}.

X-ray Crystal Structure Analysis of Complex 14 (L = PCy$_3$): $C_{41}H_{53}AuCrF_6NO_9PS_2$, $M_r = 1161.90$ g · mol^{-1}, black plate, crystal size 0.13 x 0.13 x 0.08 mm, triclinic, space group $P\bar{1}$, $a =$ 11.5038(12) Å, $b =$ 11.5987(8) Å, $c =$ 18.3790(17) Å, $\alpha =$ 78.710(7)°, $\beta =$ 84.559(8)°, $\gamma =$ 78.756(7)°, $V =$ 2354.6(4) Å^3, $T =$ 100 K, $Z = 2$, $D_{calc} =$ 1.639 g·cm^3, $\lambda =$ 0.71073 Å, μ(*Mo-K*$_\alpha$) = 3.540 mm^{-1}, Gaussian absorption correction ($T_{min} =$ 0.63, $T_{max} =$ 0.77), Bruker-AXS Enraf-Nonius KappaCCD diffractometer, $2.92 < \theta <$ 29.95°, 51488 measured reflections, 13590 independent reflections, 10643 reflections with $I > 2\sigma(I)$,

Structure solved by direct methods and refined by full-matrix least-squares against F^2 to R_1 = 0.037 [$I > 2\sigma(I)$], wR_2 = 0.076, 561 parameters, H atoms riding, S = 1.075, residual electron density 1.3 / -1.7 e Å^{-3}.

X-ray Crystal Structure Analysis of Complex 14 (L = IMes): $C_{40}H_{34}AuCrN_3O_8F_6S_2 \cdot 0.5\ C_4H_{10}O$, M_r = 1148.37 g·mol^{-1}, red prism, crystal size 0.11 x 0.09 x 0.06 mm, orthorhombic, space group $Pca2_1$, a = 16.4897(17) Å, b = 17.390(2) Å, c = 16.7386(13) Å, V = 4799.8(8) Å^3, T = 100 K, Z = 4, D_{calc} = 1.589 g·cm^3, λ = 0.71073 Å, μ(*Mo-K*$_\alpha$) = 3.441 mm^{-1}, Gaussian absorption correction (T_{min} = 0.73, T_{max} = 0.83), Bruker-AXS Enraf-Nonius KappaCCD diffractometer, 2.97 < θ < 28.96°, 26588 measured reflections, 9853 independent reflections, 6615 reflections with $I > 2\sigma(I)$. Several low-angle reflections were affected by the beam stop and removed. Structure solved by direct methods and refined by full-matrix least-squares against F^2 to R_1 = 0.047 [$I > 2\sigma(I)$], wR_2 = 0.103, 578 parameters, H atoms riding, S = 1.027, Flack parameter (absolute structure) = 0.026(7), residual electron density 2.0 / -1.4 e Å^{-3}. Intensity statistics indicate the loss of ether from the crystal lattice. The resulting local rearrangement of the structure may explain the somewhat oblate (adp max/min ratio = 4.3) atomic displacement ellipsoid for C1.

CCDC-963592 (**10**, L = IMes), **CCDC-963593** (**10**, L = PPh_3), **CCDC-963594** (**14**, L = PCy_3), **CCDC-963595** (**8**), **CCDC-963596** (**14**, L = IMes), **CCDC-963597** (**12**) contain the supplementary crystallographic data for this paper. This information can be obtained free of charge from The Cambridge Crystallographic Data Centre via www.ccdc.cam.ac.uk/data_request/cif.

General: All reactions were carried out under Ar in flame-dried glassware. The solvents were purified by distillation over the indicated drying agents under Ar: Et_2O (Mg/anthracene), CH_2Cl_2 (CaH_2), pentanes (Na/K). Flash chromatography (FC): Merck silica gel 60 (40-63 µm). NMR: Spectra were recorded on Bruker AV 400 or AV 500 spectrometers at the indicated temperatures; chemical shifts (δ) are given in ppm relative to TMS, coupling constants (J) in Hz. The solvent signals were used as references and the chemical shifts converted to the TMS scale (CD_2Cl_2: δ_C = 53.8 ppm; residual $CHDCl_2$ in CD_2Cl_2: δ_H = 5.32 ppm). ESI-MS: ESQ 3000 (Bruker), HRMS: Bruker APEX III FT-MS (7 T magnet) or MAT 95 (Finnigan). Unless stated otherwise, all commercially available compounds (Fluka, Aldrich) were used as received.

Complex 8. $(Cy_3P)AuNTf_2$ (720 mg, 0.95 mmol) is added in portions over the course of a few minutes

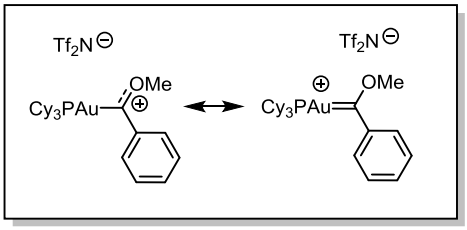

to an orange-red solution of the chromium carbene complex **7** (296 mg, 0.95 mmol)[1] in CH_2Cl_2 (3 mL), causing an immediate color change to brown. The mixture is stirred for 1 h at ambient temperature before it is cooled to −78°C. All precipitated material is filtered off under Ar at this temperature and the resulting filtrate is evaporated under reduced pressure (15 mbar). The residue is dried in vacuo (10^{-3} mbar) before it is dissolved in the minimum amount of CH_2Cl_2; layering with pentane followed by slow decrease of the temperature to −78°C with the help of a cryostat furnishes complex **8** in form of dark-red crystals suitable of X-ray analysis (498 mg, 60 %). ^{1}H NMR (400 MHz, CD_2Cl_2): δ = 8.33 (d, J = 7.7 Hz, 2 H), 7.94 (t, J = 7.2 Hz, 1 H), 7.71 (t, J = 7.6 Hz, 2 H), 5.08 (s. 3 H), 2.4 – 2.2 (m, 3 H), 2.14 – 1.7 (m, 15 H), 1.65 – 1.1 ppm (m, 15 H); ^{13}C NMR (100 MHz, CD_2Cl_2): δ = 290.7 (d, J_{PC} = 100 Hz), 141.9 (d, J_{PC} = 6.4 Hz), 140.5 (*para*-C), 135.7 (*ortho*-C), 130.3 (*meta*-C), 120.5 (J_{CF} = 321 Hz), 71.7, 33.5 (d, J_{PC} = 27.8 Hz), 31.4, 27.3 (d, J_{PC} = 11.9 Hz), 26.2 ppm; ^{31}P NMR (162 MHz, CD_2Cl_2): δ = 55.3 ppm; MS (ESI): *m/z* 597 ($M^+ - NTf_2$); HRMS (ESI): *m/z* calcd for $C_{26}H_{41}AuOP$ [$M^+ - NTf_2$]: 597.2555, found: 597.2559.

NMR inspection showed that the same reaction occurs quantitatively when performed at −50°C.

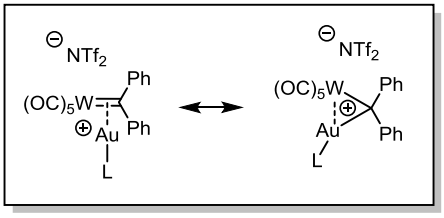

Complex 10 (L = IMes). (IMes)$AuNTf_2$ (168 mg, 0.21 mmol) is added to a solution of the tungsten carbene **9** (103 mg, 0.21 mmol)[2] in CH_2Cl_2 (2 mL) at −50°C and stirring is continued at this temperature for 5 h. Next, stirring is stopped and the reaction mixture carefully layered with cold (−50°C) pentane (3 mL). The temperature is slowly decreased to −78°C with the help of a cryostat, causing complex **10**

[1] L. S. Hegedus, M. A. McGuire, L. M. Schultze, *Org. Synth.* **1987**, *65*, 140-145.
[2] C. P. Casey, T. J. Burkhardt, C. A. Bunnell, J. C. Calabrese, *J. Am. Chem. Soc*. **1977**, *99*, 2127-2134.

(L = IMes) to crystallize from the mixture. The supernatant is removed via canula, the remaining red-black crystals are washed with cold (−78°C) pentane/CH_2Cl_2 before they are dried in vacuum (10^{-3} mbar/−30°C). (180 mg, 67 %). ^{1}H NMR (500 MHz, CD_2Cl_2, −50° C): δ = 7.47 (t, *J* = 7.3 Hz, 2 H), 7.34 (s, 2 H), 7.26 (t, *J* = 7.3 Hz, 4 H), 6.98 (s, 4 H), 6.55 (d, *J* = 7.7 Hz, 4 H),2.33 (s, 6 H), 1.81 ppm (s, 12 H); ^{13}C NMR (125 MHz, CD_2Cl_2, −50° C): δ = 252.4, 207.0 (*trans*-CO), 192.9 (*cis*-CO), 188.8, 162.0, 140.4, 134.3, 133.2, 131.9, 129.4, 128.6, 127.4, 123.9, 119.5 (J_{CF} = 321 Hz), 21.0, 17.1 ppm; MS (ESI): *m/z* 963 ($M^+ - NTf_2 - CO$), 935 (963 − CO), 907 (935 − CO).

Complex 10 (L = PPh_3). (Ph_3P)AuNTf_2 (310 mg, 0.42 mmol) is added to a solution of the tungsten carbene **9** (205 mg, 0.42 mmol) in CH_2Cl_2 (3 mL) at −78°C and stirring is continued at this temperature for 2 h, during which the color of the mixture changes from dark red to yellow-brown. The mixture is then allowed to reach −20°C before stirring is discontinued and Et_2O (3 mL) is carefully introduced. The mixture is slowly cooled to −78°C with the help of a cryostat, causing complex **10** (L = PPh_3) to crystallize from the mixture. The supernatant liquid is removed via canula, the solid is carefully rinsed with cold (−78°C) pentane/CH_2Cl_2, and the remaining crystals dried in vacuum (10^{-3} mbar/−30°C) to give the title complex as red-black crystals (482 mg, 93 %). ^{1}H NMR (400 MHz, CD_2Cl_2, −80° C): δ = 7.66 (t, *J* = 7.4 Hz, 2 H), 7.60 (dt, *J* = 7.2 Hz, 2 Hz, 3 H), 7.53 – 7.44 (m, 10 H), 7.24 – 7.14 ppm (m, 10 H); ^{13}C NMR (100 MHz, CD_2Cl_2, −80° C): δ = 263.8 (d, J_{PC} = 35.6 Hz), 205.6 (J_{WC} = 107.5 Hz), 193.2 (J_{WC} = 123.2 Hz) 162.7, 133.55, 133.48 (d, J_{PC} = 14 Hz), 132.8 (J_{PC} = 2.5 Hz), 129.8 (d, J_{PC} = 12.2 Hz), 129.4, 128.5, 126.3 (d, J_{PC} = 59.3 Hz), 119.5 ppm (q, J_{CF} = 321 Hz); ^{31}P NMR (162 MHz, , CD_2Cl_2, −80° C): δ = 50.9 ppm; MS (ESI): *m/z* 921 ($M^+ - NTf_2$ – CO), 893 (921 – CO).

Complexes **10** containing ligands L other than IMes were prepared analogously using the corresponding gold complexes L$AuNTf_2$; for characteristic NMR data, see Table S-1

Table S-1. NMR data (CD_2Cl_2) of bimetallic complexes of type **10**.[a]

L	Carbene-C [$J_{P,C}$]	C_{ipso}	C_{ortho} & C_{meta}	C_{para}	CO (*cis*) [$J_{W,C}$]	CO (*trans*) [$J_{W,C}$]	CF_3 [$J_{F,C}$]	^{31}P NMR
IMes [b]	252.4	162.0	127.5, 128.6	131.9	192.9 [123]	207.0 [111]	119.5 [321]	---
PMe_3 [c]	261.5 [37]	163.3	129.1, 127.4	132.6	193.8 [124]	206.5 [108]	119.5 [321]	14.1
PCy_3 [d]	265.9 [32]	161.9	129.2, 128.6	133.2	193.6 [124]	206.4 [112]	119.4 [321]	74.3
PPh_3 [e]	262.6 [36]	162.6	129.2, 128.4	133.3	193.1 [124]	205.7 [110]	119.2 [321]	50.9

[a] shifts in ppm, coupling constants (*J*) in Hz; [b] signals of the ligand: 188.0, 140.4, 134.3, 133.2, 129.4, 123.9, 21.0, 17.1; [c] signals of the ligand [$J_{P,C}$]: 15.2 [37]; [d] signals of the ligand [$J_{P,C}$]: 32.3 [26.7], 30.2, 26.4 [12.3], 25.2; [e] signals of the ligand [$J_{P,C}$]: 133.4 [14], 132.6 [2.1], 129.5 [12.1], 126.0 [59.2].

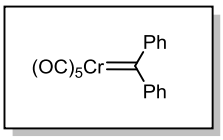

Complex 12. A solution of PhLi (1.8 M in Bu_2O, 1.3 mL, 2.34 mmol) is rapidly added at −78°C to a solution of complex **7** (692 mg, 2.15 mmol)1 in Et_2O (50 mL), causing the formation of a pale brown suspension. After stirring for another 30 min at this temperature, HCl (2 M in Et_2O, 1.3 mL, 2.6 mmol) is introduced at this temperature, causing the instantaneous formation of a dark red solution. After the mixture has reached −40°C, it is transferred via canula onto a cooled (−40°C) flash column filled with silica (h = 3 cm, Ø = 5 cm). The product is eluted with cold pentanes, the product-containing fractions are evaporated at −40°C under vacuum (10^{-3} mbar), the residue is dissolved at −30°C in cold pentane (ca. 20 mL), and the resulting solution slowly cooled to −78°C with the help of a cryostat. The supernatant liquid is removed via canula and the residue dried in vacuum (10^{-3} mbar) to afford the title complex in form of black crystals (583 mg, 76 %). Mp > 46° C (decomp.); ^{13}C NMR (100 MHz, CD_2Cl_2, −20° C): δ = 397.7, 236.1 (*trans*-CO), 216.1 (*cis*-CO), 164.0, 130.9, 127.6, 124.6 ppm.

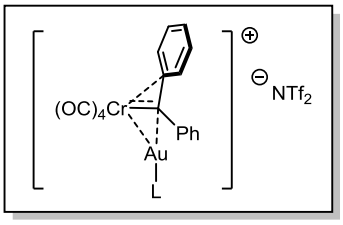

Complex 14 (L = PCy_3). $(Cy_3P)AuNTf_2$ (265 mg, 0.35 mmol) is added at −50°C to a dark-red solution of complex **12** (127 mg, 0.35 mmol) in CH_2Cl_2 (1.5 mL). The temperature is then raised to −30°C and the mixture stirred for 24 h at this temperature before it is cooled again to −78°C. The cold mixture is filtered to remove small amounts of precipitated $Cr(CO)_6$ (ca. 16 mg, identified by the characteristic ^{13}C NMR shift at δ = 212.5 ppm), and the filtrate evaporated at −30°C in vacuum (10^{-3} mbar). The remaining dark brown residue (289 mg, containing ca. 75% of **14** by ^{31}P NMR) is recrystallized by slowly cooling a solution in Et_2O (1.5 mL) from −30°C to −78°C with the help of a cryostat to give the title complex in form of green crystals suitable for X-ray diffraction. ^{1}H NMR (400 MHz, CD_2Cl_2, −80° C): δ = 8.20 (d, *J* = 7.8 Hz, 1 H), 7.97 (t, *J* = 7.1 Hz, 1 H), 7.87 (t, *J* = 8.1 Hz, 1 H), 7.81 (t, *J* = 7.5 Hz, 1 H), 7.55 (m, 2 H), 7.46 (m, 2 H), 7.05 (d, *J* = 7 Hz, 1 H), 7.03 (d, *J* = 7 Hz, 1 H), 2.10 – 1.93 (m, 3 H), 1.93 – 1.49 (m, 15 H), 1.47 – 0.92 ppm (m, 15 H); ^{13}C NMR (100 MHz, CD_2Cl_2, −80° C): δ = 243.2 (d, *J* = 48 Hz), 231.9, 228.0, 224.4, 222.8, 144.2, 138.7 (d, J_{PC} = 1.9 Hz), 137.8, 137.6, 134.3, 129.9, 129.8, 129.5, 129.0, 128.0, 126.9 (d, J_{PC} = 1.9 Hz), 126.6, 119.1 (q, J_{CF} = 321 Hz), 93.6, 31.6 (d, J_{PC} = 27.2), 30.0 (2C), 26.2 (d, J_{PC} = 12 Hz), 25.0 ppm; ^{31}P NMR (162 MHz, CD_2Cl_2, −80° C): δ = 72.5 ppm.

When the reaction is performed in CD_2Cl_2 and monitored by NMR (−50°C), the formation of complex **14** is preceded by formation of a transient complex, to which structure **13** is tentatively assigned based on the characteristic NMR signals [^{13}C NMR: δ = 307.3 ppm ($J_{P,C}$ = 33 Hz); ^{31}P NMR: δ = 71.7 ppm] and by analogy to the tungsten series; after 4 h at −50°C, the ratio **13**/**14** = 57:43 (^{31}P NMR); after stirring at −30°C for 24 h, the characteristic signal of **13** is no longer detected.

Complexes **13** and **14** containing ligands L other than PCy_3 were prepared analogously using the corresponding gold complexes $LAuNTf_2$; for characteristic NMR data, see Table S-2

Table S-2. Characteristic NMR data (CD_2Cl_2) of bimetallic complexes of types **13** and **14**.[a]

L	X	13		14		
		Carbene-C [$J_{P,C}$]	**^{31}P NMR**	**Carbene-C [$J_{P,C}$]**	**C_{ipso}**	**^{31}P NMR**
PCy_3	NTf_2	307.3 [33]	71.7	243.1 [47]	93.6	72.6
	SbF_6	306.4 [33]	71.9	243.0 [48]	93.6	72.4
PMe_3	NTf_2	303.3 [39]	9.5	235.0 [61]	94.0	16.8
PPh_3	NTf_2	305.4 [39]	47.1	238.7 [55]	93.6	51.6
IMes	NTf_2	n.d.		232.2	94.9	

[a] shifts in ppm, coupling constants (*J*) in Hz

Computational Section

Computational Methods:

Geometry optimizations were carried out using the BP86 functional[1,2] in combination with the def2-TZVP basis set.[3] For the gold atom, the 60 inner-shell core electrons were replaced by an effective core potential (ECP) generated for the neutral atom using quasi-relativistic methods.[4] The remaining explicitly treated electrons were described using the corresponding def2-ECP basis set. Additionally the empirical Grimme-type dispersion corrections were also incorporated using the latest parametrization (D3).[5] The resolution of identity (RI) approximation[6-8] was employed for efficient computation. This computational setup had already proved to be efficient and reliable for the study of gold complexes.[9-11] The located stationary points were characterized as minima by evaluating the harmonic vibrational frequencies computed at the same level (RI-BP86/def2-TZVP+D3). These computations were performed using the TURBOMOLE suite of programs (version 6.3).[12, 13]

In order to get insight into the electronic structure of the complexes, a Natural Population Analysis (NPA) was carried out at RI-BP86/def2-TZVP+D3 level. The Wiberg bond indices for selected bonds were evaluated at BP86/LANL2DZ level using the NBO code version 3.1[14] as implemented in the Gaussian 09 suite of programs.[15] Additionally, a fragment analysis was performed using the Amsterdam Density Functional (ADF) program package.[16-18] In this analysis, the complexes are built from user-defined fragments. The molecular orbitals of the fragments are expanded in terms of Slater-type orbitals (STOs), employing a triple-ζ basis set with one polarization function (TZP). The resulting symmetrized fragment orbitals (SFOs) are used as new basis functions to recompute the electronic structure of the complexes. These calculations were also corrected for relativistic effects using the zero-order regular approximation (ZORA) approach.[19, 20]

The Atoms-in-Molecule (AIM) analysis[21] was performed based on the geometries optimized at the BP86/def2-TZVP level (with an effective core potential for Au as described above). For the generation of the wave function, a single-point Gaussian 09 calculation was run (B3LYP/6-311+G** with SDD basis set and pseudopotential for Au). The AIM calculation itself was done by using AIMAll.[22] The AIM analysis allows the identification of bonds between atoms based on the gradient of the electron density. The characteristic bond critical points are defined as saddle points where the gradient of the electron density is zero in all directions and its second derivatives are negative in two directions and positive in the direction of the bound atoms.[21]

Isotropic chemical shielding constants were computed within the GIAO ansatz.[23] Besides the GGA functional chosen for the optimization (BP86) we also applied the hybrid functional B3LYP as recommended.[24] For calculations performed with Turbomole, a smaller basis had to be applied due

to technical reasons (def2-SVP for Au, C, H, O, P; def2-TZVP for Cr and C1, C_{ipso}, C'_{ipso}; corresponding core potential for Au). To include relativistic effects chemical shieldings were calculated using ADF as well (BP86/TZP, no core potentials). To perform calculations with larger basis sets, Gaussian 09 was employed choosing the SDD basis set and potential for Au and the 6-311+G** basis set for all other atoms.

References

1. A. D. Becke, *Phys. Rev. A* **1988**, *38*, 3098-3100.
2. J. P. Perdew, *Phys. Rev. B* **1986**, *33*, 8822-8824.
3. F. Weigend, R. Ahlrichs, *Phys. Chem. Chem. Phys.* **2005**, *7*, 3297-3305.
4. D. Andrae, U. Häussermann, M. Dolg, H. Stoll, H. Preuss, *Theor. Chim. Acta* **1990**, *77*, 123-141.
5. S. Grimme, J. Antony, S. Ehrlich, H. Krieg, *J. Chem. Phys.* **2010**, *132*, 154104.
6. K. Eichkorn, O. Treutler, H. Öhm, M. Häser, R. Ahlrichs, *Chem. Phys. Lett.* **1995**, *242,* 652-660.
7. K. Eichkorn, F. Weigend, O. Treutler, R. Ahlrichs, *Theor. Chem. Acc.* **1997**, *97*, 119-124.
8. F. Weigend, *Phys. Chem. Chem. Phys.* **2002**, *4*, 4285-4291.
9. S. Flügge, A. Anoop, R. Goddard, W. Thiel, A. Fürstner, *Chem. Eur. J.* **2009**, *15*, 8558-8565.
10. M. Alcarazo, T. Stork, A. Anoop, W. Thiel, A. Fürstner, *Angew. Chem. Int. Ed*. **2010**, *49*, 2542-2546.
11. H. Teller, M.Corbet, L. Mantilli, G. Gopakumar, R. Goddard, W. Thiel, A. Fürstner, *J. Am. Chem. Soc.* **2012**, *134*, 15331-15342.
12. R. Ahlrichs, M. Bär, M. Häser, H. Horn, C. Kölmel, *Chem. Phys. Lett.* **1989**, *162*, 165-169.
13. TURBOMOLE V6.3 **2011**, a development of University of Karlsruhe and Forschungszentrum Karlsruhe GmbH, 1989-2007, TURBOMOLE GmbH, since 2007; available from www.turbomole.com
14. NBO Version 3.1, E. D. Glendening, A. E. Reed, J. E. Carpenter, F. Weinhold.
15. Gaussian 09, Revision B.01, M. J. Frisch, G. W. Trucks, H. B. Schlegel, G. E. Scuseria, M. A. Robb, J. R. Cheeseman, G. Scalmani, V. Barone, B. Mennucci, G. A. Petersson, H. Nakatsuji, M. Caricato, X. Li, H. P. Hratchian, A. F. Izmailov, J. Bloino, G. Zheng, J. L. Sonnenberg, M. Hada, M. Ehara, K. Toyota, R. Fukuda, J. Hasegawa, M. Ishida, T. Nakajima, Y. Honda, O. Kitao, H. Nakai, T. Vreven, J. A. Montgomery Jr., J. E. Peralta, F. Ogliaro, M. Bearpark, J. J. Heyd, E. Brothers, K. N. Kudin, V. N. Staroverov, R. Kobayashi, J. Normand, K. Raghavachari, A. Rendell, J. C. Burant, S. S. Iyengar, J. Tomasi, M. Cossi, N. Rega, J. M. Millam, M. Klene, J. E. Knox, J. B. Cross, V. Bakken, C. Adamo, J. Jaramillo, R. Gomperts, R. E. Stratmann, O. Yazyev, A. J. Austin, R. Cammi, C. Pomelli, J. W. Ochterski, R. L. Martin, K. Morokuma, V. G. Zakrzewski, G. A. Voth, P. Salvador, J. J. Dannenberg, S. Dapprich, A. D. Daniels, Ö. Farkas, J. B. Foresman, J. V. Ortiz, J. Cioslowski, D. J. Fox, Gaussian, Inc., Wallingford CT, **2010**.
16. C. Fonseca Guerra, J. G. Snijdres, G. te Velde, E. J. Baerends *Theor. Chem. Acc.* **1998**, *99*, 391-

403.

17. G. te Velde, F. M. Bickelhaupt, E. J. Baerends, C. Fonseca Guerra, S. J. A. van Gisbergen, J. G. Snijders, T. Ziegler, *J. Comput. Chem.* **2001**, *22*, 931-967.

18. ADF 2012.01, SCM, Theoretical Chemistry, Vrije Universiteit Amsterdam, The Netherlands, **2012**; www.scm.com

19. E. van Lenthe, E. J, Baerends, J. G. Snijders, *J. Chem. Phys.* **1994**, *101*, 9783.

20. E. van Lenthe, A. E. Ehlers, E. J. Baerends, *J. Chem. Phys.* **1999**, *110*, 8943.

21. R. F. W. Bader, *Acc. Chem. Res.* **1985**, *18*, 9-15.

22. AIMAll Version 13.05.06, T. A. Keith, TK Gristmill Software, Overland Park KS, USA, **2013**; aim.tkgristmill.com

23. K. Wolinski, J. F. Hinton, P. Pulay, *J. Am. Chem. Soc.* **1990**, *112*, 8251-8260.

24. M. Bühl, T. van Mourik, *WIREs Comput. Mol. Sci.* **2011**, *1*, 634-647.

Computational Results:

We have applied Density Functional Theory (DFT) to study the electronic structure of complexes **13** and **14** (see main paper). The optimized geometries of these complexes are illustrated in Figures S-7 and S-8, respectively. They are in good agreement with the X-ray structures, as can be seen from the comparison of selected calculated and experimental geometrical parameters in Tables S-3 and S-4.

Table S-3. Selected bond lengths in complex **14** [experimental (X-ray structure) vs. calculated (RI-BP86/def2-TZVP+D3)].

bond	**bond length in Å experimental**	**bond length in Å calculated**
Au-P	2.331	2.340
Au-C1	2.136	2.171
Au-Cr	2.718	2.720
C1-Cr	1.993	1.979
C1-C_{ipso}	1.469	1.470
C1-C'_{ipso}	1.476	1.460
Cr-C_{ipso}	2.272	2.330

Table S-4. Selected bond angles in complexes **13** and **14** at the RI-BP86/def2-TZVP+D3 level.

angle	**13**	**14**
P-Au-Cr	151.1	158.3
P-Au-C1	157.7	155.7
C1-Au-Cr	51.2	46.1
Cr-C1-O	172.6	175.9
CO-Cr-CO	169.3	85.7
C_{ipso}-C1-C'_{ipso}	113.3	121.8
Cr-C1-C_{ipso}	127.1	83.6

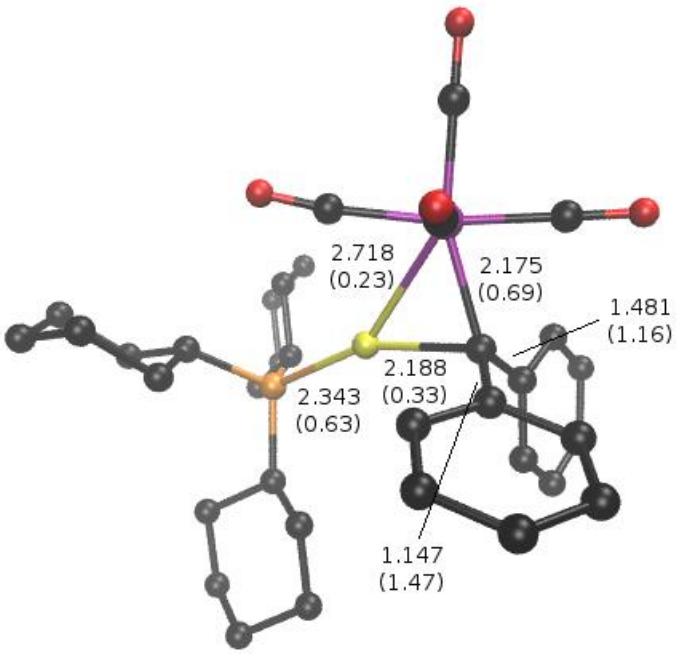

Figure S-7 Optimized geometry of complex **13** at RI-BP86/def2-TZVP+D3 level. The hydrogen atoms are omitted for clarity (color code: black=carbon, violet=chromium, yellow=gold, red=oxygen, orange=phosphorous). Selected bond length (Å) and Wiberg bond indices (in parentheses) are also given.

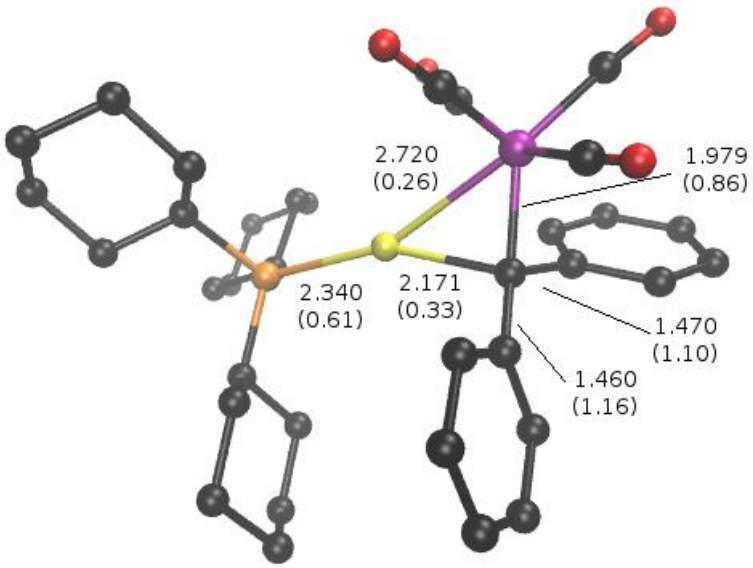

Figure S-8 Optimized geometry of complex **14** at RI-BP86/def2-TZVP+D3 level. The hydrogen atoms are omitted for clarity (color code: black=carbon, violet=chromium, yellow=gold, red=oxygen, orange=phosphorous). Selected bond length (Å) and Wiberg bond indices (in parentheses) are also given.

Fragment analysis. In order to gain insight into the electronic structure of the complexes, a fragment molecular orbital analysis has been performed. In this analysis, the molecule is built from user-defined fragments. For each of them, fragment orbitals (FOs) are calculated starting from atomic orbitals (AOs). These FOs are used as new basis functions to recompute the molecular orbitals (MOs) of the full complexes. We have adopted two different fragment analysis schemes for complexes **13** and **14**. In the first one (fragmentation A), the complex after full geometry optimization is divided into a $[P(Cy)_3Au]^+$ fragment and a $[C(Ph)_2Cr(CO)_n]$ fragment. In the second scheme (fragmentation B), the complex is divided into a $[Cr(CO)_n]$ fragment and a $[C(Ph)_2P(Cy)_3Au]^+$ fragment (see Scheme S-1). MOs are generated for each of these fragments, and the total electronic structure is then recomputed based on the fragment orbitals. In this way it is possible to determine the contributions of the fragment orbitals to the MOs of the corresponding complex.

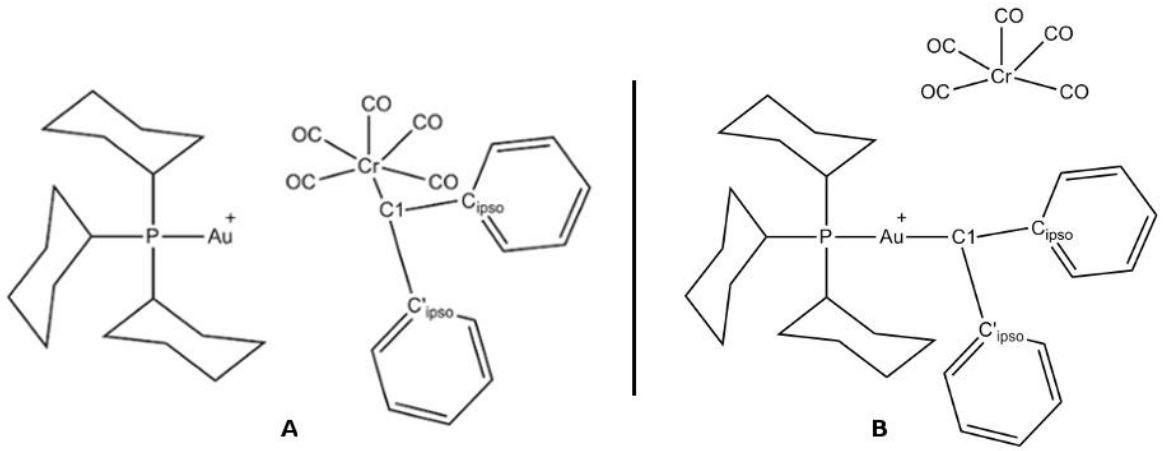

Scheme S-1 Representation of the two fragmentation schemes adopted for complex **13**.

Fragmentation A. The gross populations of the FOs (from LUMO+1 to HOMO-3) in complexes **13** and **14** are listed in Tables S-5 and S-6, respectively, and the shapes of selected FOs of complex **14** are represented in Figure S-9. We adopted the selection criterion that the population of the FO had to change by at least ±0.1 electrons upon recombination. The lowest unoccupied molecular orbital (LUMO) of the gold fragment, which has a large contribution from the 6s atomic orbital of the metal atom ($\%s_{Au}$=44), receives 0.51 and 0.45 electrons in case of complex **13** and **14**, respectively. The charge is donated mainly from the HOMO-1 of the $[C(Ph)_2Cr(CO)_5]$ fragment in case of complex **13**, and from the HOMO and HOMO-1 of the $[C(Ph)_2Cr(CO)_4]$ fragment in case of complex **14** (see Tables S-5 and S-6). The main contributions from FOs (single contribution larger than 0.1) to the orbitals LUMO to HOMO-3 are given in Table S-7 for both complexes. Please note that the MOs resulting from the interaction of fragment orbitals have large contributions from the $[C(Ph)_2Cr(CO)_5]$ fragment.

In case of complex **13**, HOMO-1 and HOMO-3 of the $[C(Ph)_2Cr(CO)_5]$ fragment contribute 48% and 17%, respectively, while there are only minor contributions from the HOMO-2 (8%) and the LUMO (6%) of the $[P(Cy)_3Au]^+$ fragment. In case of complex **14**, HOMO-1 and HOMO of the $[C(Ph)_2Cr(CO)_4]$ fragment contribute 43% and 11%, respectively, while there is only 7% contribution from the LUMO of the $[P(Cy)_3Au]^+$ fragment. Hence, as there is no strong orbital mixing between the $[P(Cy)_3Au]^+$ and $[C(Ph)_2Cr(CO)_n]$ fragments, the bonding situation can be described as a chromium-carbene complex with a weakly coordinating gold unit (η^2 binding mode). This is also well reflected in the very low Wiberg bond indices derived for these bonds (see Figures S-7 and S-8).

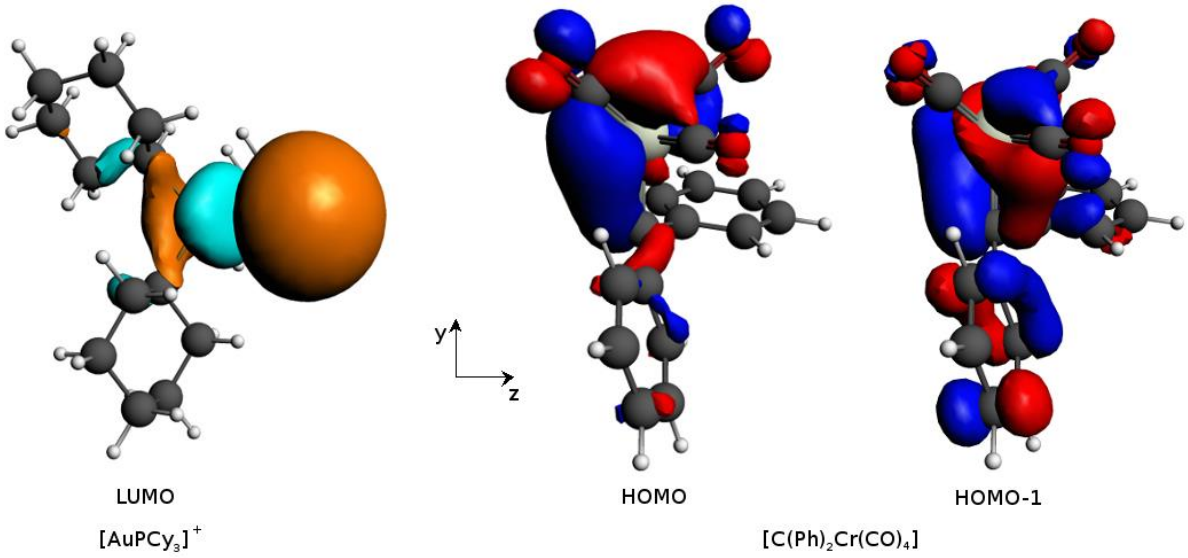

Figure S-9 Shape of selected fragment orbitals (fragmentation A) of complex **14** at BP86/TZP(ZORA) level. The local axis frame chosen for the analysis is also specified in the figure.

Table S-5. Fragment analysis of complex **13** (fragmentation A). The gross populations (summation over all MOs) of frontier fragment orbitals are given at BP86/TZP(ZORA) level. The dominant AO contributions are mentioned if they are mainly localized at Au, Cr or C1.

Orbitals of $[AuPCy_3]^+$ fragment	**SFO gross populations**	**Orbitals of $[C(Ph)_2Cr(CO)_5]$ fragment**	**SFO gross populations**
LUMO+1 ($6p_y$)	0.06	LUMO+1	0.02
LUMO (6s)	0.51	LUMO (C1 $2p_y$)	0.15
HOMO	2.00	HOMO (Cr $3d_{xz}$)	1.98
HOMO-1	1.99	HOMO-1 (π)	1.70
HOMO-2 (6s/5d)	1.92	HOMO-2 (Cr $3d_{x2-z2}$)	1.99
HOMO-3	2.00	HOMO-3 (σ)	1.96

Table S-6. Fragment analysis of complex **14** (fragmentation A). The gross populations (summation over all MOs) of frontier fragment orbitals are given at BP86/TZP(ZORA) level. The main AO contributions are mentioned if they are mainly localized at Au, Cr or C1.

Orbitals of $[AuPCy_3]^+$ fragment	FO gross populations	Orbitals of $[C(Ph)_2Cr(CO)_4]$ fragment	FO gross populations
LUMO+1 ($6p_y$)	0.05	LUMO+1	0.03
LUMO (6s)	0.45	LUMO (C1 $2p_y$)	0.11
HOMO	2.00	HOMO (Cr $3d_{xz}$)	1.82
HOMO-1	1.99	HOMO-1 (π)	1.85
HOMO-2 (6s/5d)	1.96	HOMO-2 (Cr $3d_{x2-y2}$)	1.99
HOMO-3	2.00	HOMO-3 (σ)	1.97

Table S-7. Contributions of fragment orbitals (fragmentation scheme A, contributions larger than 0.1) to molecular orbitals of both complexes, respectively.

molecular orbital	complex 13	complex 14
LUMO	0.86 LUMO $[C(Ph)_2Cr(CO)_5]$	0.85 LUMO $[C(Ph)_2Cr(CO)_4]$
HOMO	0.95 HOMO $[C(Ph)_2Cr(CO)_5]$	0.66 HOMO, 0.27 HOMO-1 $[C(Ph)_2Cr(CO)_4]$
HOMO-1	0.48 HOMO-1, 0.17 HOMO-3 $[C(Ph)_2Cr(CO)_5]$	0.87 HOMO-2 $[C(Ph)_2Cr(CO)_4]$
HOMO-2	0.86 HOMO-2 $[C(Ph)_2Cr(CO)_5]$	0.47 HOMO-1, 0.11 HOMO $[C(Ph)_2Cr(CO)_4]$
HOMO-3	0.61 HOMO-3, 0.11 HOMO-1 $[C(Ph)_2Cr(CO)_5]$	0.40 HOMO-2 $[AuPCy_3]^+$, 0.23 HOMO-3, 0.15 HOMO-6 $[C(Ph)_2Cr(CO)_4]$

Fragmentation B. The gross populations of the frontier FOs (LUMO+1 through HOMO-3) in complexes **13** and **14** are listed in Tables S-8 and S-9, respectively, and the shapes of selected FOs of complexes **13** and **14** are represented in Figures S-10 and S-11, respectively. Again, we include all fragment frontier orbitals with a change of population of at least ±0.1 electrons upon recombination to form the MOs of the full complexes. The LUMO of fragment $[AuPCy_3C(Ph)_2]^+$ has large

contributions from the $2p_z$ orbital of C1 (39% and 44% in complex **13** and **14**, respectively). Additionally, the LUMO+1 of this fragment has small contributions from the 2p orbital of both ipso carbon atoms (around 10% each for C2 and C8). In the case of complex **13**, the HOMO of the $[AuPCy_3C(Ph)_2]^+$ fragment has large contributions from the $2p_y$ orbital located at C1 (20%) with a minor contribution from the $5d_{xz}$ orbital at Au (5%). Correspondingly, for complex **14** the main contributions to the HOMO arise from a $2p_y$ orbital located at C1 (19%) complemented by minor contributions from the 6s orbital located at Au (7%). For both complexes, the HOMO-1 is mainly localized around Au, with main contributions from 6s (23-26%) and 5d (14-19%). In both complexes, this fragment receives electrons from the HOMO of the $[Cr(CO)_n]$ fragment, and at the same time there is a considerable amount of back-donation to the LUMO of the latter fragment (cf. Tables S-8 and S-9). The resulting MOs have contributions from both fragments. The main contributions (larger than 0.1) of FOs to the orbitals LUMO up to HOMO-3 are listed in Table S-10 for both complexes. The HOMO-1 of complex **13** has the following contributions from the respective FOs: 39% from the HOMO of the $[Cr(CO)_5]$ fragment, 15% from the LUMO of the $[AuPCy_3C(Ph)_2]^+$ fragment. Similarly the HOMO-3 of complex **13** has main contributions from the HOMO of the $[AuPCy_3C(Ph)_2]^+$ fragment (65%) and from the LUMO and the HOMO-1 of the chromium fragment (4% each).

For complex **14**, the LUMO has the following contributions from the respective FOs: 49% from the LUMO of $[AuPCy_3C(Ph)_2]^+$ fragment, 24% from the HOMO of the chromium fragment. The HOMO-2 of complex **14** has mainly contributions from the HOMO and HOMO-2 of $[Cr(CO)_4]$ (25% and 24%, respectively) and the LUMO+1 of $[AuPCy_3C(Ph)_2]^+$ (19%). This clearly indicates σ-bonding/π-backbonding interactions between the chromium and carbene units in both complexes, which are also reflected in the electron transfers between these fragments (Tables S-8 and S-9). The Wiberg bond indices (Figures S-7 and S-8) also suggest strong bonding interactions between Cr and C1. By contrast, according to the orbital interaction analysis and the Wiberg bond indices (WBI), there are no significant bonding interactions between Cr and C_{ipso} in complex **13** (WBI = 0.02) and also not in complex **14** (WBI=0.15) despite the fact that the C_{ipso} atom is much closer to Cr in complex **14**.

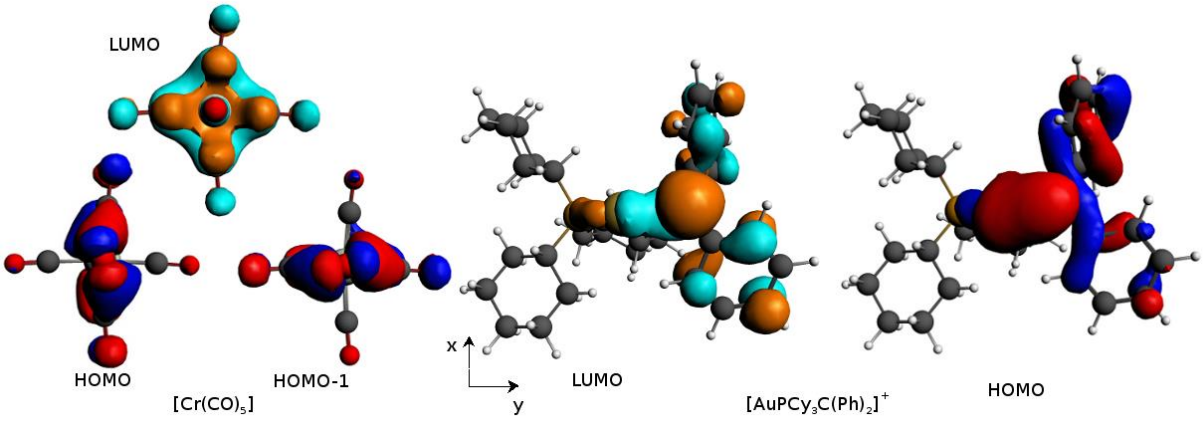

Figure S-10 Shape of selected fragment orbitals (fragmentation B) of complex **13** at BP86/TZP(ZORA) level. The local axis frame chosen for the analysis is also specified in the figure.

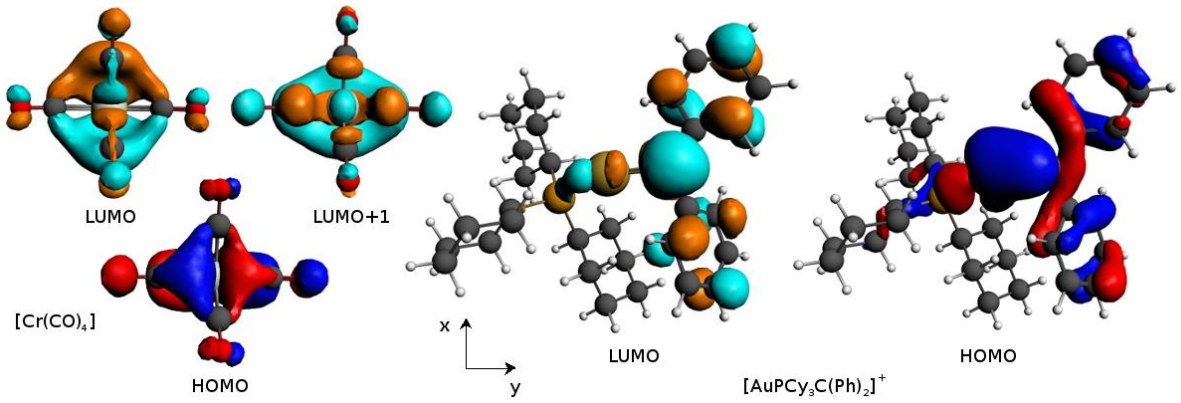

Figure S-11 Shape of selected fragment orbitals (fragmentation scheme B) of complex **14** at BP86/TZP(ZORA) level. The local axis frame chosen for the analysis is also specified in the figure.

Table S-8. Fragment analysis (fragmentation scheme B) of complex **13**: The gross populations (summed over all MOs) of frontier fragment orbitals are given at BP86/TZP level.

Orbitals of $[AuPCy_3C(Ph)_2]^+$ fragment	**FO gross populations**	**Orbitals of $[Cr(CO)_5]$ fragment**	**FO gross populations**
LUMO+1	0.00	LUMO+1	0.01
LUMO (C1 $2p_z$)	0.49	LUMO ($3d_{z2}$)	0.40
HOMO (C1 $2p_y$)	1.73	HOMO ($3d_{xz}$)	1.59
HOMO-1 (Au 6s/5d)	1.96	HOMO-1 ($3d_{yz}$)	1.86
HOMO-2	2.00	HOMO-2 ($3d_{xy}$)	1.99
HOMO-3	2.00	HOMO-3	1.99

Table S-9. Fragment analysis (fragmentation B) of complex **14**: The gross populations (summation over all MOs) of frontier fragment orbitals are given at BP86/TZP level.

Orbitals of $[AuPCy_3C(Ph)_2]^+$ fragment	FO gross populations	Orbitals of $[Cr(CO)_4]$ fragment	FO gross populations
LUMO+1	0.04	LUMO+1 ($3p_z$)	0.25
LUMO (C1 $2p_z$)	0.71	LUMO ($3d_{xy}$)	0.39
HOMO (C1 $2p_y$)	1.63	HOMO ($3d_{xz}$)	1.28
HOMO-1 (Au 6s/5d)	1.98	HOMO-1 ($3d_{x2-y2}$)	1.96
HOMO-2	2.00	HOMO-2 ($3d_{yz}$)	1.96
HOMO-3	1.99	HOMO-3	1.99

Table S-10. Contributions of fragment orbitals (fragmentation B, contributions larger than 0.1) to molecular orbitals of both complexes.

molecular orbital	complex 13	complex 14
LUMO	0.64 LUMO $[AuPCy_3C(Ph)_2]^+$, 0.14 HOMO $[Cr(CO)_5]$	0.49 LUMO $[AuPCy_3C(Ph)_2]^+$, 0.24 HOMO $[Cr(CO)_4]$
HOMO	0.75 HOMO-1, 0.12 HOMO $[Cr(CO)_5]$	0.91 HOMO-1 $[Cr(CO)_4]$
HOMO-1	0.39 HOMO, 0.14 HOMO-2 $[Cr(CO)_5]$, 0.15 LUMO $[AuPCy_3C(Ph)_2]^+$	0.61 HOMO-2, 0.15 HOMO $[Cr(CO)_4]$
HOMO-2	0.76 HOMO-2 $[Cr(CO)_5]$	0.25 HOMO, 0.24 HOMO-2 $[Cr(CO)_4]$, 0.19 LUMO $[AuPCy_3C(Ph)_2]^+$
HOMO-3	0.65 HOMO $[AuPCy_3C(Ph)_2]^+$	0.69 HOMO-1 $[AuPCy_3C(Ph)_2]^+$

Dissociation energies. The energies required to separate the complexes **13** and **14** into the respective fragments are listed in Table S-11 for fragmentation schemes A and B. The energy of the fragments was computed at the geometry that they adopt in the complex (no relaxation). For complex **13**, the computed energies are similar for fragmentation schemes A and B, while there are considerable differences in the case of complex **14** where the dissociation of the Cr-C1 bond (*i.e.,* fragmentation B) into frozen fragments requires more energy than that of the Au-Cr/C1 bond. This implies a strong Cr-C1 bonding interaction in complex **14**.

Table S-11. Dissociation energies(kcal/mol) of the complexes into frozen fragments (no relaxation) at BP86/TZP(ZORA) level.

	fragmentation A	**fragmentation B**
complex 13	42.44	39.09
complex 14	49.44	63.76

AIM analysis. For further characterization of the bonding, we performed a topological analysis of the electron density distribution using the Atoms-in-Molecules (AIM) method. This method identifies bonds between atoms through so-called bond critical points (*i.e.*, saddle points of the electron density, where the gradient is zero in all directions while the second derivatives are positive along the bond and negative in the two other orthogonal directions). The resulting bond network (with bond critical points indicated as green dots) and the associated density contour maps are shown in Figures S-12 and S-13 for complex **13** and in Figures S-14 and S-15 for complex **1**, respectively.

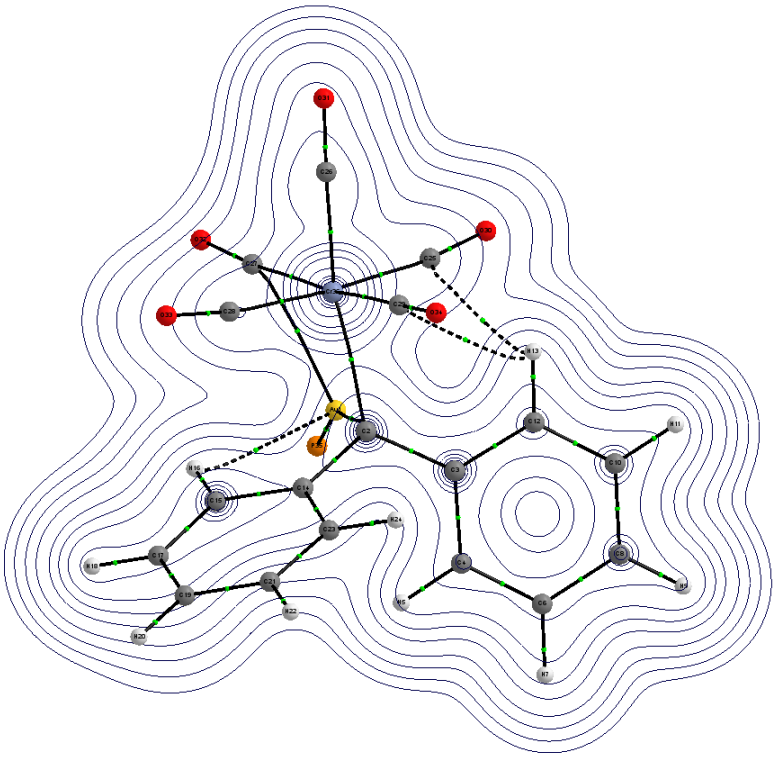

Figure S-12 Graphical representation of bond critical points (green dots) and the electron density contour map in the plane C1, Cr, C_{ipso} as obtained by the AIM method for complex **13**. The ligands at phosphorous are left out for clarity.

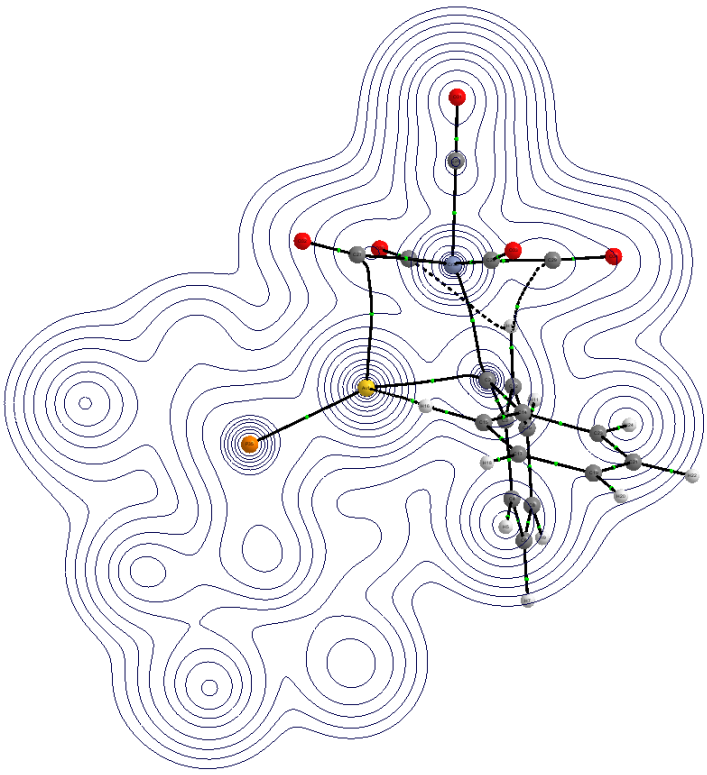

Figure S-13 Graphical representation of bond critical points (green dots) and the electron density contour map in the plane Au, C1, Cr as obtained by the AIM method for complex **13**. The ligands at phosphorous are left out for clarity.

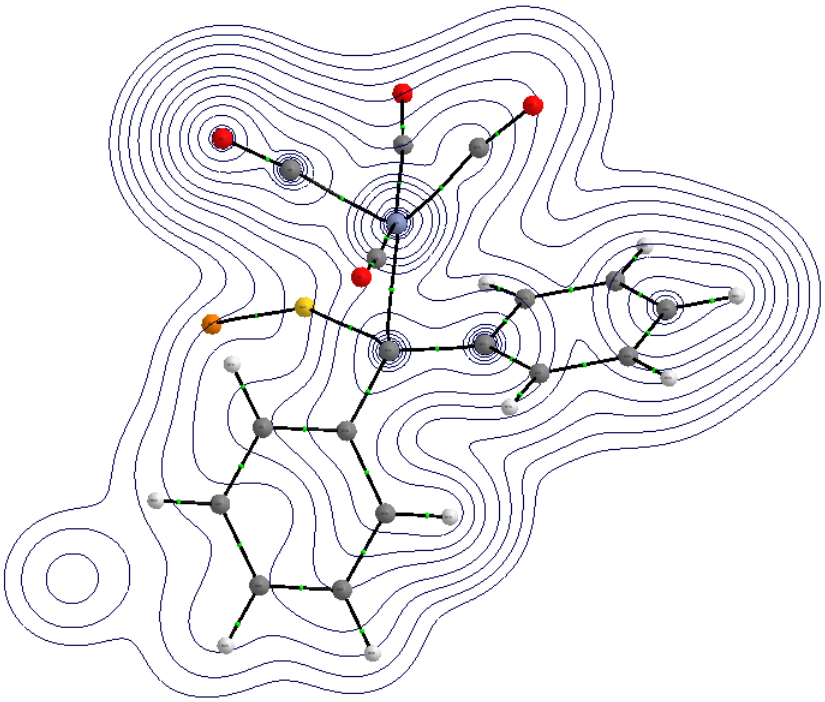

Figure S-14 Graphical representation of bond critical points (green dots) and the electron density contour map in the plane C1, Cr, C_{ipso} as obtained by the AIM method for complex **14**. The ligands at phosphorous are left out for clarity.

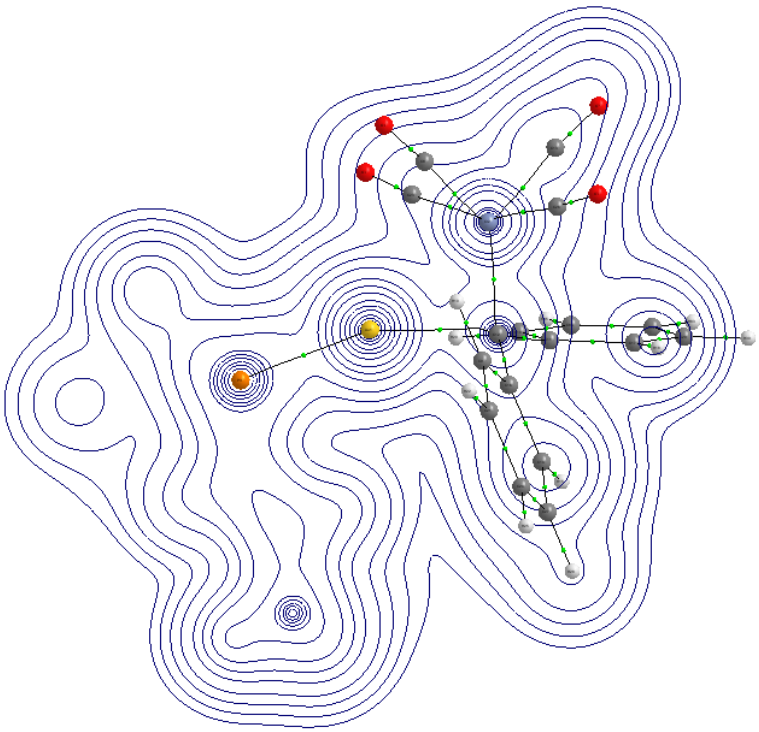

Figure S-15 Graphical representation of bond critical points (green dots) and the electron density contour map in the plane Au, C1, Cr as obtained by the AIM method for complex **14**. The ligands at the phosphorous are left out for clarity.

One should be cautious, however, not to over-interpret the AIM results. It is known that the AIM method may have difficulties to identify bridging bonding interactions. In the present case, the AIM analysis finds a bond critical point between Au and the carbene carbon atom C1 in both complexes (see Figures S-13 and S-15). There is no separate nearby bond critical point between Au and Cr, since the electron density distribution indicates only one bonding path that is directed more towards C1 than to Cr. Moreover, for complex **13** the AIM analysis provides an unexpected bond critical point between Au and a carbonyl group (see Figure S-13), which is in contrast to the low NBO Wiberg bond index of 0.15 and the lack of a distinct orbital interaction in the fragment analysis.

NMR chemical shifts. Experimentally, the NMR chemical shifts have been measured for C_{ipso} and C'_{ipso} in complex **14**. We have calculated these shifts using several computational procedures (for different density functionals and basis sets, without and with inclusion of relativistic effects). The NMR chemical shifts δ are obtained from the computed isotropic shielding constants σ by $\delta = \delta_{ref} + \sigma_{ref} - \sigma$.

As in the experimental work, dichloromethane was chosen as reference. We computed σ_{ref} at the same level as σ, and δ_{ref} was taken from experiment.

Table S-12. Isotropic shielding constants and isotropic chemical shifts calculated at various levels for C_{ipso} and C'_{ipso} in complex **14** (geometry optimized at the BP86/def2-TZVP level).

	functional	**basis set**	**ECP (Au)**	**relativistic**	**Isotropic shielding constant σ /ppm**			**Isotropic chemical shift δ / ppm**		
					CH_2Cl_2	C_{ipso}	C'_{ipso}	C_{ipso}	C'_{ipso}	$\delta_{C'ipso}$-δ_{Cipso}
	experimental							93	144	51
1	BP86*	def2-SVP	def2-ecp	no	118.77	92.99	46.84	79.58	125.73	46.15
2	BP86*	[1]	def2-ecp	no	103.95	83.30	33.76	74.45	123.99	49.55
3	B3LYP*	[1]	def2-ecp	no	106.38	80.34	29.68	79.84	130.50	50.66
4	BP86#	TZP	none	no	108.29	84.49	41.14	77.60	120.95	43.35
5	BP86#	TZP	none	Spin-orbit coupling	114.52	84.04	38.20	84.28	130.12	45.84
6	BP86$	[2]	SDD	no	107.45	82.80	33.72	78.46	127.53	49.08
7	B3LYP$	[2]	SDD	no	109.55	79.79	29.26	83.56	134.09	50.53

* Turbomole, # ADF, $ Gaussian, various basis sets: [1] Cr, C_{ipso}, C'_{ipso}, C1 def2-TZVP, others def2-SVP; [2] Au SDD, others 6-311+G**

It is obvious from Table S-12 that the differences between the NMR chemical shifts of C_{ipso} and C'_{ipso} are well reproduced by all computational methods used, with C_{ipso} being remarkably shielded. The shifts themselves are generally underestimated. As expected, the agreement between the calculated and experimental shifts improves upon going from the GGA functional BP86 to the hybrid functional B3LYP (see entries 2 and 3, or entries 6 and 7), upon extending the basis set (see entries 3 and 7), and upon including relativistic corrections (see entries 4 and 5). To provide a best estimate for the NMR shifts, we add to our best non-relativistic result (entry 7) the relativistic corrections (differences of

entries 5 and 4), which yields 90.24 ppm for C_{ipso}, 143.26 ppm for C'_{ipso}, and 53.02 ppm for the difference, in good agreement with the experimental values (see Table S-12). The electronic structure obtained from the DFT calculations is thus consistent with the experimental NMR data.

Conclusion. The gold moiety is a weakly bound unit in both complexes: the Cr-C1 bond coordinates in η^2-fashion to the gold moiety. A relatively weak bonding interaction is also seen from the small Wiberg bond indices calculated for the Au-Cr and Au-C1 bonds. The strong Cr-C1 bonding arises from simultaneous σ-donation and π-back-donation, with strong mixing of the respective fragment orbitals. Finally, even though C_{ipso} gets much closer to the chromium atom upon removal of a carbonyl ligand, there is no significant bonding interaction between these two atoms both according to orbital analysis (NBO, fragmentation) and topological analysis of the electron density (AIM).

Cartesian coordinates of the optimized geometries (RI-BP86/def2-TZVP+D3, Å)

13

au	0.7302726684	-1.0310238798	0.0109890198
c	2.6578325889	-1.7189143476	-0.7636935316
c	3.5703053182	-0.8553323329	0.0196037837
c	3.8644463056	0.4458992967	-0.4826992828
h	3.4428575588	0.7546710733	-1.4384445970
c	4.6450983022	1.3395321463	0.2428584441
h	4.8386130292	2.3349785019	-0.1578731396
c	5.1906082316	0.9580605371	1.4715879428
h	5.8176263815	1.6514160251	2.0329517058
c	4.9359035392	-0.3238464515	1.9753782937
h	5.3771701020	-0.6360120310	2.9221240377
c	4.1286686269	-1.2084867815	1.2714292366
h	3.9642166940	-2.2042010585	1.6753397072
c	2.8197392935	-1.5680916714	-2.2196959198
c	1.7174456209	-1.4705516543	-3.0996478683
h	0.7078363172	-1.4994710641	-2.6867023943
c	1.9068842562	-1.3182865966	-4.4678520737
h	1.0442133110	-1.2173417555	-5.1265445329
c	3.2012088003	-1.3200766499	-5.0008517006
h	3.3484836526	-1.2312315179	-6.0775749574
c	4.3055294181	-1.4473565973	-4.1509818266
h	5.3141538321	-1.4664998033	-4.5646872524
c	4.1220109042	-1.5427106546	-2.7752925691
h	4.9842195957	-1.6369219912	-2.1147344292
c	1.6910041739	-3.1154887663	1.7478877042
c	1.5021857538	-5.3491754499	0.4655136570
c	-0.2105065274	-3.4800332286	-0.1713078980
c	1.5867450258	-4.1893159497	-1.9085737381
c	3.5668023927	-3.9720879302	-0.1777910582
o	1.6148425859	-2.9424729978	2.8877436063
o	1.3793189178	-6.4298383858	0.8420231510
o	-1.3612082831	-3.5776532896	-0.2295416607
o	1.4783565569	-4.6714914595	-2.9479903065
o	4.6818127948	-4.2450958517	-0.2655788416
p	-0.9611395652	0.4878921659	0.5761632013
cr	1.7110486962	-3.5631705163	-0.1067095651
c	-2.5762722907	-0.2774106862	0.0754980830
c	-3.8718485755	0.3815358999	0.5873051217
c	-2.6279471320	-0.5043627529	-1.4501840843

h	-2.5054749600	-1.2735361582	0.5503757021
c	-5.0867674387	-0.4760106536	0.1964306027
h	-3.9825500861	1.3869605277	0.1566037659
h	-3.8397447345	0.5026699134	1.6785439571
c	-3.8517121452	-1.3486618504	-1.8307263142
h	-2.6814736952	0.4687053612	-1.9641225402
h	-1.7037766787	-0.9962790399	-1.7943722724
c	-5.1484794252	-0.7122660799	-1.3168563877
h	-6.0067840016	0.0124052905	0.5500453082
h	-5.0251599127	-1.4468491185	0.7171792927
h	-3.8883180837	-1.4740261432	-2.9230196884
h	-3.7367382476	-2.3568780790	-1.3987876137
h	-6.0095424226	-1.3482054813	-1.5682415065
h	-5.3098105119	0.2524003459	-1.8293311994
c	-0.6512082716	2.1276769060	-0.2453391744
c	0.0983280167	1.9881889401	-1.5879966630
c	-1.8860076491	3.0345907970	-0.4140710106
h	0.0400840133	2.6141521042	0.4709550046
c	0.5028195399	3.3644589843	-2.1318472601
h	-0.5502549257	1.4772450824	-2.3189139367
h	0.9876958569	1.3502433167	-1.4618903650
c	-1.4707916619	4.4129875570	-0.9497828717
h	-2.5791461194	2.5662831877	-1.1317086444
h	-2.4333692245	3.1438125578	0.5315473146
c	-0.7088565892	4.2932169532	-2.2739284877
h	1.0134410912	3.2436192694	-3.0990061781
h	1.2353495000	3.8204819924	-1.4428277821
h	-2.3645841970	5.0422282325	-1.0729739663
h	-0.8341192405	4.9149684204	-0.2005751177
h	-0.3897915307	5.2858160415	-2.6232588258
h	-1.3866617096	3.8915298414	-3.0474452380
c	-0.9250118459	0.7593333683	2.4137637094
c	-1.6633853463	2.0000919714	2.9520858747
c	-1.3479644351	-0.5256352257	3.1562774869
h	0.1540749927	0.9127366938	2.6034717496
c	-1.4530598637	2.1271420351	4.4699987014
h	-2.7401594451	1.9232897048	2.7382848287
h	-1.3020053812	2.9114176003	2.4532620268
c	-1.1395885202	-0.3742601234	4.6692709616
h	-2.4128986614	-0.7316991280	2.9585612775
h	-0.7802718489	-1.3914240787	2.7796535376
c	-1.8788341536	0.8545586225	5.2112760148
h	-2.0103734527	2.9988197775	4.8438486556
h	-0.3860351093	2.3268444203	4.6696723171
h	-1.4771404002	-1.2880617868	5.1798512236
h	-0.0601075039	-0.2777905622	4.8759358326

h	-1.6960007593	0.9641170101	6.2901227444
h	-2.9663716933	0.7085591390	5.0905616858

14

au	-0.9623828021	0.0730797898	0.5587486478
cr	-3.3188240133	0.0861616443	1.9167843527
p	0.4887595501	0.0145633667	-1.2761662718
o	-3.8439320314	-2.3163034985	0.1935962816
o	-3.7184806812	-2.0701203924	4.0017671501
o	-3.9950057255	1.6019697552	-0.6767562166
o	-6.0284063524	1.0392948747	2.9039128888
c	-3.6649352788	-1.3796999516	0.8538358180
c	-0.3865190507	-2.0802868046	3.0097957396
h	-1.1462220198	-2.5356051154	2.3727754392
c	-1.9522635964	1.3886455504	3.2819241424
c	-1.4872770912	0.1381181314	2.6646475142
c	-5.0246291084	0.6456469475	2.4983648000
c	0.5294222430	-0.1163970659	4.1149712619
h	0.4921401323	0.9532496602	4.3238239594
c	-0.4623906664	-0.6944221247	3.2882440573
c	-2.2960778199	1.4132091125	4.6685844486
h	-2.0891965482	0.5300672519	5.2741758392
c	-2.2546035700	2.5382201891	2.5028243487
h	-1.8826344790	2.5926497976	1.4803426159
c	0.6317837321	-2.8569677262	3.5482391937
h	0.6698948629	-3.9254399445	3.3360947885
c	-3.6986611248	1.0867195541	0.3099396453
c	1.6093953606	-2.2665836254	4.3592955244
h	2.4142113704	-2.8750258957	4.7727587838
c	-3.5464305371	-1.2253809112	3.2336235051
c	1.5566735984	-0.8960237896	4.6376180379
h	2.3215307852	-0.4370579908	5.2645142518
c	-2.9146186033	2.5164813536	5.2231175333
h	-3.1814809016	2.5134343211	6.2800535099
c	2.1558371247	-0.5293813763	-0.6740783058
c	2.7839686007	0.5230783888	0.2608181846
c	2.0595138399	-1.9001699975	0.0274556371
h	2.7911561990	-0.6303499093	-1.5706139989
c	4.1432424505	0.0500168659	0.7960179298
h	2.1007486610	0.7024540177	1.1110549715
h	2.9064039387	1.4840496012	-0.2604154399
c	3.4230418265	-2.3567525398	0.5624064287
h	1.3541960573	-1.8187803964	0.8727345231
h	1.6475879352	-2.6584847975	-0.6540759786

c	4.0313035990	-1.3073828684	1.4975991012
h	4.5501698431	0.8091985022	1.4805086715
h	4.8544360288	-0.0288504597	-0.0442399235
h	3.3051211753	-3.3192285102	1.0829425990
h	4.1078848501	-2.5388062408	-0.2832977559
h	5.0184149038	-1.6359764315	1.8540338786
h	3.3882808962	-1.2039235820	2.3893780076
c	-0.0607511242	-1.1315299681	-2.6380217964
c	1.0924864834	-1.7391603973	-3.4639407789
c	-1.0189185828	-2.2326690846	-2.1373912555
h	-0.6406104858	-0.4637518090	-3.3014748049
c	0.5375833366	-2.5641980962	-4.6359216801
h	1.6960091327	-2.3993396742	-2.8206523805
h	1.7676970049	-0.9567944393	-3.8377483405
c	-1.5543462276	-3.0680138316	-3.3081735591
h	-0.4856515001	-2.8905194399	-1.4304186422
h	-1.8549821081	-1.7852885490	-1.5789624162
c	-0.4154613467	-3.6606161374	-4.1464083979
h	1.3733643677	-3.0011052014	-5.2023538398
h	0.0026030281	-1.8931367589	-5.3296390258
h	-2.2088049735	-3.8631094512	-2.9219326515
h	-2.1837096043	-2.4257174206	-3.9477280826
h	-0.8222781975	-4.2213582863	-5.0003380843
h	0.1489564909	-4.3856163867	-3.5345216217
c	0.6819503743	1.7030487860	-2.0149342450
c	1.6982712726	1.7879941480	-3.1679581052
c	-0.6783919691	2.2965880841	-2.4331070907
h	1.0621824392	2.3079435056	-1.1716508086
c	1.8599445965	3.2430220988	-3.6355345844
h	1.3389605354	1.1784508611	-4.0136393890
h	2.6729602969	1.3760512933	-2.8651269842
c	-0.5128658862	3.7466418686	-2.9113133837
h	-1.1104224548	1.6954328838	-3.2512090421
h	-1.3929965237	2.2465121111	-1.5968314277
c	0.5135707969	3.8513148273	-4.0457607237
h	2.5739813251	3.2843570100	-4.4712833508
h	2.2991293201	3.8380868778	-2.8161165331
h	-1.4875348138	4.1414839816	-3.2337575277
h	-0.1842730873	4.3699476330	-2.0613073722
h	0.6451145624	4.9014279590	-4.3444582364
h	0.1298321945	3.3188983701	-4.9331456077
c	-3.2275507998	3.6352469903	4.4240706423
h	-3.7243411272	4.4964681434	4.8717118570
c	-2.8962413992	3.6469846181	3.0765019192
h	-3.1146129100	4.5191161504	2.4607972308